

Experimental demonstration of guiding and confining light in nanometer-size low-refractive-index material

Qianfan Xu, Vilson R. Almeida, Roberto R. Panepucci, and Michal Lipson

School of Electrical and Computer Engineering, Cornell University, 411 Phillips Hall, Ithaca, New York 14853

Received February 8, 2004

We experimentally demonstrate a novel silicon waveguide structure for guiding and confining light in nanometer-wide low-refractive-index material. The optical field in the low-index material is enhanced because of the discontinuity of the electric field at high-index-contrast interfaces. We measure a 30% reduction of the effective index of light propagating in the novel structure due to the presence of the nanometer-wide low-index region, evidencing the guiding and confinement of light in the low-index material. We fabricate ring resonators based on the structure and show that the structure can be implemented in highly integrated photonics.

© 2004 Optical Society of America
OCIS codes: 130.3120, 130.2790.

Guiding light in low-index materials such as air is thought to be prohibited in conventional waveguides based on total internal reflection. Instead, external reflections from multiple dielectric layers^{1,2} or photonic crystals³ are usually employed. However, these structures are wavelength sensitive and have relatively large dimensions to provide high reflections. We recently showed that the optical field can be enhanced and confined in a low-refractive-index material even when light is guided by total internal reflection.⁴ The proposed structure is a low-index nanometer-wide area embedded in a high-index material medium. In contrast with the leaky modes used in photonic bandgap waveguides with low-index cores, the guiding mode is an eigenmode of the proposed structure and is therefore fundamentally lossless with very low wavelength sensitivity.⁴

The proposed waveguiding structure, called a slot waveguide, is shown in Fig. 1(a). The waveguide consists of a nanometer-wide low-index (n_S) slot embedded between two rectangular high-index (n_H) regions, both surrounded by a low-index (n_C) cladding. The principle of operation is based on the discontinuity of the normal component of the electric field at the high-index-contrast interface⁴; the major component of the electric field of the quasi-TE mode (E_x) is perpendicular to the walls of the slot, thereby undergoing strong discontinuity at the walls, with much higher amplitude in the low-index slot [see Fig. 2(a)]. The ratio between the values of E_x at both sides of the walls is equal to the square of the index ratio across the wall (n_H^2/n_S^2), which equals 12 for an air slot embedded between two silicon regions. When the dimensions of the slot are smaller than the decay length of the field from the interface into the low-index region, the electric field remains high within the slot. The magnetic field is continuous at the walls of the slot; therefore the optical intensity in the slot is much higher than that in the high-index region. The power transmitted in a sub-100-nm-wide low-index slot can be higher than 40% of the total power when the slot waveguide is optimally designed. For the quasi-TM mode, with the major component of the electric field parallel to the

walls of the slot, the effect of the presence of the slot is minimal.

We fabricated the slot waveguide on a silicon-on-insulator (SOI) wafer with a 3- μm buried oxide layer by electron-beam lithography patterning, followed by inductively coupled plasma etching and deposition of a 3- μm -thick SiO_2 cladding by plasma-enhanced chemical-vapor deposition. Figure 1(b) shows a scanning electron microscopy (SEM) top-view picture of the slot waveguide before the SiO_2 cladding is deposited. We measured the parameters of the waveguide to be $w_H = 220 \pm 10$ nm, $w_S = 100 \pm 10$ nm, and $h = 250 \pm 10$ nm. The refractive indices of the silicon and the silicon oxide are assumed to be $n_H = 3.48$ and $n_C = 1.46$, respectively. Because of the low temperature, the narrow slot is not filled with SiO_2 in the plasma-enhanced chemical-vapor deposition process. We simulated the eigenmodes of the fabricated structure by use of a full-vectorial finite-difference mode solver⁵ with a nonuniform grid mesh, taking the refractive index in the slot as $n_S = 1$. The simulated transverse electric field distribution of the quasi-TE mode is shown in Fig. 2(a). In the figure, one can clearly see the field discontinuities at index-contrast interfaces and the strong field confinement in the slot.

To show experimentally that the optical power for the quasi-TE mode is indeed concentrated in the air slot, one needs to measure the effective index of the slot waveguide eigenmode. We expect the effective index to be much lower than that of a conventional channel

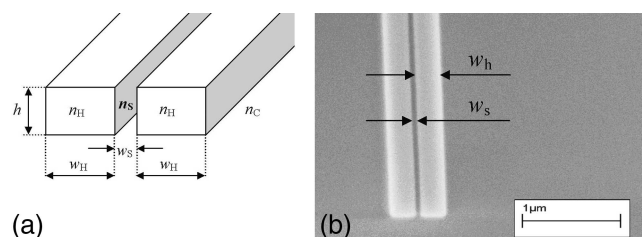


Fig. 1. (a) Schematic of the slot waveguide. (b) Top-view SEM picture of the slot waveguide before deposition of the SiO_2 upper cladding.

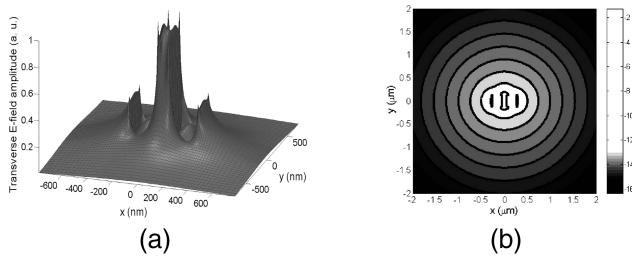


Fig. 2. Transverse electric field of the quasi-TE mode in a SOI-based slot waveguide, when $w_h = 218$ nm, $w_s = 101$ nm, $h = 247$ nm, $n_H = 3.48$, $n_S = 1$, and $n_C = 1.46$. The dimensions are estimated from the cross-sectional SEM picture of the fabricated device. The origin of the coordinate system is located at the center of the waveguide, with a horizontal x axis and a vertical y axis. (a) Three-dimensional profile of the field amplitude. (b) Two-dimensional contours of the logarithm of the normalized field amplitude.

waveguide. The effective index can be obtained from the decay rate γ of the optical field in the cladding far from the center of the slot waveguide, assuming that the decay is exponential with respect to radial distance r to the center. Given the decay rate γ , the effective index of the mode is

$$n_{\text{eff}} \approx (n_C^2 + \gamma^2/k_0^2)^{1/2}, \quad (1)$$

where k_0 is the vacuum wave number. The assumption of the exponential decay of the field is verified in the simulation; Fig. 2(b) shows the contours of the logarithm of transverse electric-field amplitude E for the quasi-TE mode. At a sufficiently large distance ($r > 1 \mu\text{m}$) from the center of the slot waveguide the contours are almost circular and equally spaced, indicating that $E(r)$ indeed decays exponentially with r as $E(r) \propto \exp(-\gamma r)$.

To obtain the experimental value of the effective index by measuring the decay rate γ , we fabricated directional couplers, each composed of two parallel slot waveguides, with different separation distances d . Figure 3 shows a SEM picture of a typical directional coupler. Coupling coefficient κ is proportional to the overlap of the electric field of both slot waveguides.⁶ Therefore decay rate γ is related to coupling coefficient κ between the two parallel slot waveguides as $\kappa(d) \propto \exp(-\gamma d)$. The coupling coefficient is in turn related to power ratio K between the output power (P_{o2}) of one slot waveguide and the input power (P_{in}) in the parallel slot waveguide (see Fig. 3) as $K(d) = P_{o2}/P_{\text{in}} = \sin^2[\kappa(d)L]$, where L is the length of the directional coupler. Therefore

$$\ln \kappa(d) = \ln\{\arcsin[K(d)]^{1/2}/L\} = -\gamma d + C, \quad (2)$$

where C is a constant independent of d . Decay rate γ , and therefore effective index n_{eff} , can then be obtained from the experimentally measured K -versus- d relationship with a linear fit. In our experiment we

measured the power-coupling ratio K for different values of d at different wavelengths for both quasi-TE and quasi-TM modes and obtained the effective indices at each wavelength.

We show the experimental results of the effective indices for both the quasi-TE mode and the quasi-TM mode in Fig. 4 (crosses and diamonds, respectively). We also show the simulated dispersion curves obtained with the full-vectorial finite-difference mode solver (solid curve for quasi-TE mode and dashed curve for quasi-TM mode). One can see good agreement between the simulated and the experimental results. The simulated dispersion curves when there is no slot, i.e., $w_s = 0$, are also shown in Fig. 4 (solid and dashed curves for quasi-TE and quasi-TM modes, respectively). When no slot is present, the effective index of the quasi-TE mode ($n_{\text{eff}} \sim 2.4$) is much higher than that of the quasi-TM mode, indicating that the power of the quasi-TE mode is mostly confined in the silicon core. When the slot is introduced, a strong decrease in the effective index of the quasi-TE mode is measured ($n_{\text{eff}} \sim 1.6$), whereas the effective index of the quasi-TM mode is only slightly affected. This behavior is direct evidence that, for the quasi-TE mode, light is indeed concentrated in the low-index region because of the field discontinuity.

The slot waveguide can be implemented in highly integrated photonics because of its strong confinement

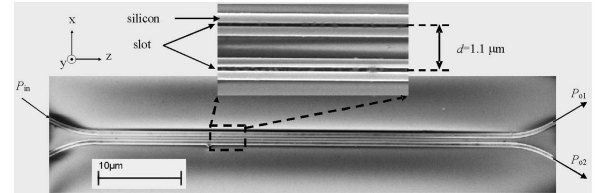


Fig. 3. Top-view SEM picture of a directional coupler formed by two parallel slot waveguides fabricated on a SOI platform. The picture was taken before deposition of the SiO_2 upper cladding.

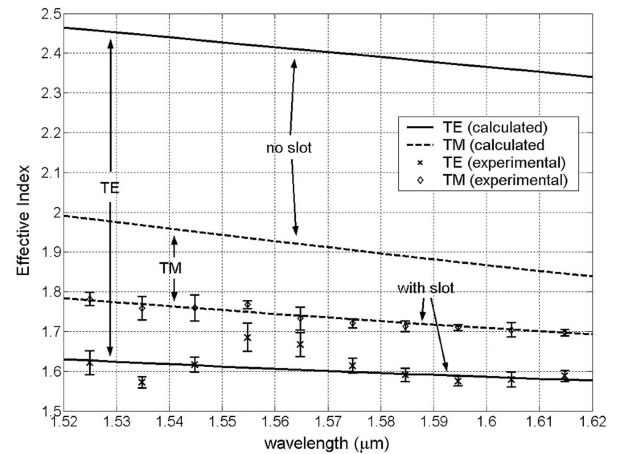


Fig. 4. Measured (marks with error bars) and simulated (curves) effective indices of quasi-TE and quasi-TM modes in a conventional and a slot waveguide. The parameters of the slot waveguide used in the simulations are the same as those in Fig. 2, except that $w_s = 0$ for the conventional channel waveguide.

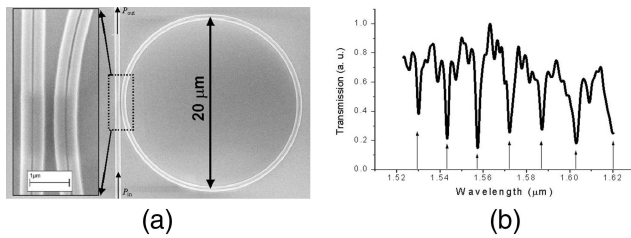


Fig. 5. (a) SEM picture of the slot waveguide ring resonator coupled to a straight slot waveguide. The coupling region is enlarged in the inset. The picture is taken before the deposition of the SiO₂ upper cladding. (b) Transmission spectrum (P_{out}/P_{in}) of the coupled slot ring resonator. The positions of the resonances are marked by arrows.

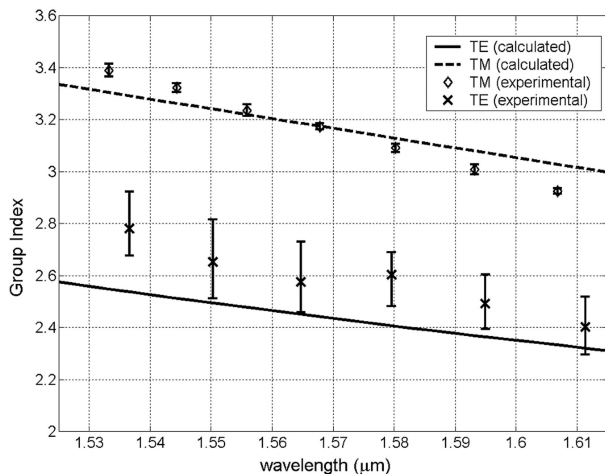


Fig. 6. Measured (marks with error bars) and simulated (curves) group indices of quasi-TE and quasi-TM modes of the slot waveguide. The parameters of the slot waveguide used in the simulation are the same as those in Fig. 2.

nature. To demonstrate the integration capabilities of the slot waveguides, we fabricated ring resonators composed of slot waveguides. A SEM picture of a straight slot waveguide coupled to a slot waveguide ring resonator is shown in Fig. 5(a). We show the transmission spectrum of the structure for the quasi-TE mode in Fig. 5(b). The resonance pattern in the measured transmission spectrum is an indication of the guiding of light in the ring. From the transmission spectrum we estimate that the Q factor of the ring resonator is ~ 1000 near the wavelength of 1550 nm. In Fig. 6 we show the group indices at different wavelengths for both the quasi-TE and the quasi-TM modes (crosses and diamonds, respectively) obtained from the transmission spectra.⁷ We also show the simulated group index spectra for both quasi-TE and quasi-TM modes of the slot waveguide forming the ring (solid and dashed curves, respectively). The simulation is based on the full-vectorial finite-difference mode solver. Relatively good agreement is obtained between the experimental and the

simulated values. The small discrepancy for the quasi-TE mode is due mainly to the bending of the waveguide, which is not taken into account in the simulation, and the uncertainty in the fabricated slot waveguide dimensions and indices, such as the exact profile of the index of refraction in the slot region due to the deposition method of the SiO₂ cladding.

In conclusion, we have shown experimental evidence that light is confined in the low-index material by use of a slot waveguide configuration, opening the opportunity for guiding and confining in novel materials with low refractive index. We show that a slot waveguide can be integrated on silicon chips, allowing compact optical sensing, optical amplification, and optical switching devices to be monolithically integrated with electronic circuits.

The authors thank Christina Manolatu for her guidance and assistance in the simulations and Stefan Preble and Bradley Schmidt for their help with the fabrication of the devices. This work was supported in part by the Science and Technology Centers program of the National Science Foundation (NSF) under agreement DMR-0120967 and by the Air Force Office of Scientific Research under grant AFOSR F49620-03-1-0424. V. R. Almeida acknowledges sponsorship support provided by the Brazilian Defense Ministry. This work was performed in part at the Cornell NanoScale Science & Technology Facility (a member of the National Nanofabrication Users Network), which is supported by the NSF under grant ECS-9731293, its users, Cornell University, and industrial affiliates. This work made use of the Cornell Center for Materials Research Shared Experimental Facilities, supported through the NSF Materials Research Science and Engineering Center program (DMR-0079992). Q. Xu's e-mail address is qx23@cornell.edu.

References

1. S. G. Johnson, M. Ibanescu, M. Skorobogatiy, O. Weisberg, T. D. Engeness, M. Soljagic, S. A. Jacobs, J. D. Joannopoulos, and Y. Fink, *Opt. Express* **9**, 748 (2001), <http://www.opticsexpress.org>.
2. H. Schmidt, Y. Dongliang, and A. Hawkins, in *Integrated Photonics Research*, Postconference Digest Vol. 91 of OSA Trends in Optics and Photonics Series (Optical Society of America, Washington, D.C., 2003), paper ItuC2.
3. R. F. Cregan, B. J. Mangan, J. C. Knight, T. A. Birks, P. St. J. Russel, P. J. Roberts, and D. C. Allan, *Science* **285**, 1537 (1999).
4. V. R. Almeida, Q. Xu, C. A. Barrios, R. R. Panepucci, and M. Lipson, *Opt. Lett.* **29**, 1209 (2004).
5. C. L. Xu, W. P. Huang, M. S. Stern, and S. K. Chaudhuri, *IEEE Proc. Optoelectron.* **141**, 281 (1994).
6. C. R. Pollock, *Fundamentals of Optoelectronics* (Richard D. Irwin, Burr Ridge, Ill., 1995).
7. S. Morasca, F. Pozzi, and C. De Bernardi, *IEEE Photon. Technol. Lett.* **5**, 40 (1993).